Available online at www.sciencedirect.com
ScienceDirect
Journal of Solid State Chemistry 181 (2008) 863–870
JOURNAL OF SOLID STATE CHEMISTRY
www.elsevier.com/locate/jssc

# Comparisons between surfactant-templated mesoporous and conventional sol–gel-derived $CaO–B_2O_3–SiO_2$ glasses: Compositional, textural and in vitro bioactive properties

Tongping Xiu[a,b], Qian Liu[a,*], Jiacheng Wang[a,b]

[a]*State Key Laboratory of High Performance Ceramics and Superfine Microstructure, Shanghai Institute of Ceramics, 1295 Dingxi Road, Shanghai 200050, PR China*
[b]*Graduate School of the Chinese Academy of Sciences, 19A Yuquan Road, Beijing 100039, PR China*

Received 10 October 2007; received in revised form 31 December 2007; accepted 7 January 2008
Available online 11 January 2008

**Abstract**

Compositional, textural and in vitro bioactive comparisons between surfactant-templated mesoporous (MCBS) and conventional sol–gel-derived $CaO–B_2O_3–SiO_2$ (CBS) glasses are studied in this paper. CBS glasses are heterogeneous in composition. Due to the heterogeneity, melting boron oxide that formed during the heat treatment will fill in the pores that should have been generated by decomposition of calcium species. So, unlike other conventional sol–gel-derived bioactive glasses that have disordered and widely distributed mesopores, the CBS glasses are almost nonporous. MCBS glasses are more homogeneous in composition than CBS glasses, mainly ascribed to the effect of the surfactant. MCBS glasses of different compositions possess wormhole-like mesoporous structure and have similar pore size. In vitro bioactive tests show that wormhole-like MCBS glasses are more bioactive than CBS glasses, due to their high porosity.


*Keywords:* Mesoporous materials; Surfactant-templated; Sol–gel; In vitro bioactivity

## 1. Introduction

Since the pioneering work by Hench et al. in 1972, bioactive glasses and glass-ceramics have attracted much attention [1]. When these glass or glass-ceramics are implanted in the human body, a biologically active apatite layer is formed on their surface. Subsequently, the bioactive materials spontaneously bond to and integrate with living bone [2–4]. In vivo implanting experiments showed that these bioactive glasses with certain compositions present no local or systemic toxicity, no inflammation, no foreign-body response, and bond to both soft and hard tissue without an intervening fibrous layer [2,5].

The behavior that apatite is formed on biomaterials in simulated body fluid (SBF) is known as the in vitro bioactivity, an important evaluation for the in vivo bioactivity of such bone-forming biomaterials [6]. CaO and $SiO_2$ are reported to be two important compositions in bioactive materials. CaO is dissolved to raise supersaturation of $Ca^{2+}$ in SBF and $SiO_2$ is hydrated to provide nucleation sites for apatite layer [7]. The melt-derived $CaO–B_2O_3–SiO_2$ glass and glass-ceramics have been reported to be bioactive and biodegradable [8–10]. The introduction of $B_2O_3$ into the $CaO–SiO_2$ system is expected to enhance the bioactivity, for more soluble boric compounds increase the supersaturation of Ca ions in the SBF solution and water-corrosive borosilicate glass forms Si–OH groups that act as nucleation sites for the apatite layer [11].

In addition to the classic melt-derived route, an alternative sol–gel technique was introduced to the preparation of bioactive glasses in the early 1990s [12,13]. The utilization of sol–gel method has led to a wide range of compositions and the biomaterials can be prepared under quite mild conditions [14]. However, there has been

*Corresponding author. Fax: +86 21 5241 3122.
*E-mail address:* qianliu@sunm.shcnc.ac.cn (Q. Liu).

0022-4596/$ - see front matter © 2008 Elsevier Inc. All rights reserved.
doi:10.1016/j.jssc.2008.01.012

controversy about the homogeneity of the sol–gel glasses [14,15]. It was reported that textural properties (pore size, pore volume, pore structure) of biomaterials may have complex influences on the development of the apatite layer. Increasing the specific surface area and pore volume of bioactive glasses may greatly accelerate the apatite formation and therefore enhance the bioactive behavior [14]. Wormhole-like mesoporous materials have high specific surface areas, uniform channel diameters and short-range hexagonal-like packed channels [16–18]. Furthermore, channel branching within the framework greatly facilitates access to reactive sites on the framework walls [19,20]. So, it is of great interest to compare the compositional, textural and in vitro bioactive properties of wormhole-like glasses with conventional sol–gel-derived glasses.

Recently, we have reported a novel kind of in vitro bioactive wormhole-like mesoporous $CaO–B_2O_3–SiO_2$ (MCBS) glasses prepared by a combination of surfactant templating, sol–gel method and evaporation-induced self-assembly (EISA) processes [21]. This synthesis strategy produces bioactive glasses with uniform and controllable pore sizes, relatively large pore volumes, and more importantly, high in vitro bone-forming bioactivities. In this paper, we studied in detail the comparisons between MCBS and conventional sol–gel CBS glasses in compositional, textural and in vitro bioactive properties.

## 2. Experimental

### 2.1. Sample preparation

MCBS glasses with different compositions were synthesized by using nonionic block copolymers $EO_{20}PO_{70}EO_{20}$ (P123) as structure-directing agents (EO is poly(ethylene oxide), PO is poly(propylene oxide)). In a typical synthesis of MCBS, P123 (1.0 g), tetraethyl orthosilicate (TEOS; 2.2 g), $Ca(NO_3)_2 \cdot 4H_2O$ (0.42 g), different amount of tributyl borate (TBB), and 0.5 m HCl (0.36 g) were dissolved in ethanol (20 g) and stirred at room temperature for 1 day. The resulting sol was introduced into a Petri dish to undergo an EISA process. The dried gel was calcined at 873 K for 5 h to obtain the final MCBS products (denoted $MC_xBS_y$, $x$ and $y$ refers to the molar fraction of CaO and $SiO_2$ multiplied by 100 in the initial composition, respectively). In addition, for comparison, conventional CBS glasses with the same composition was also synthesized by a route similar to the MCBS glasses synthesis method described above through a solvent evaporation process except that no surfactant was utilized (denoted $C_xBS_y$).

### 2.2. In vitro bioactivity test

The bone-forming bioactivity of MCBS and CBS in vitro was tested by immersing ground granules (100 mg) in SBF (100 mL) at 36.5 °C to monitor the formation of hydroxyapatite HAp on the surface of glasses over time, ranging from 0 to 120 h. The SBF contains 142.0 mM $Na^+$, 5.0 mM $K^+$, 1.5 mM $Mg^{2+}$, 2.5 mM $Ca^{2+}$, 147.8 mM $Cl^-$, 4.2 mM $HCO_3^-$, 1.0 mM $HPO_4^{2-}$, and 0.5 mM $SO_4^{2-}$. Its chemical composition is similar to that of human plasma and has a pH of 7.3–7.4. The powders were separated by filtration, washed with deionized water, and dried in air. Then Ca, Si, P concentration change in SBF was measured by ICP methods.

### 2.3. Characterization

Fourier-transform infrared (FTIR) spectroscopic investigations were carried out on a Bruker Vector 22 spectrometer using the KBr pellet method. Nitrogen adsorption–desorption isotherms were measured on a Micromeritics ASAP2010 surface area and pore size analyzer at liquid nitrogen temperature (77 K). Prior to measurements, the samples were dehydrated at 373 K and then outgassed at 473 K in vacuum for 4 h. The Brunauer–Emmett–Teller (BET) method was utilized to calculate the specific surface areas ($S_{BET}$). The pore volume ($V_{BJH}$) and the mean pore size ($D_{BJH}$) were derived from the adsorption branches of the isotherms using the Barrett–Joyner–Halanda (BJH) method. High-resolution transmission electron microscopy (HRTEM) images were obtained using a JEOL 2010CX TEM operated at 200 kV. Wide- and small-angle X-ray powder diffraction (WAXRD and SAXRD) patterns were collected on a Rigaku D/MAX-c β instrument using Cu$K\alpha_1$ ($\lambda = 0.15406$ nm) radiation at 40 kV and 60 mA. Scanning electron microscopy (SEM) observations were carried out on JEOL JSM-6700F working at 15 kV. The solution obtained by filtration was analyzed by inductive coupled plasma (ICP) atomic emission spectroscopy. Differential thermal analysis (DTA) and thermo-gravimetric analysis (TG) curves were recorded under dynamic air flow at a heating rate of 10 K $min^{-1}$ on crushed bulk specimen from room temperature to 1173 K. Boron was quantitated by titration as the mannitol–boric acid complex using standardized NaOH solution as titrant, whereas silicon was determined using potassium fluosilicate volumetric methods.

## 3. Results and discussions

### 3.1. Comparison of compositional homogeneity

#### 3.1.1. WAXRD

Amorphous nature of the two glasses is demonstrated by WAXRD study. Fig. 1 shows that no diffraction peaks can be observed except a broad band between 18° and 40° ($2\theta$) for MCBS glasses, which is due to the amorphous borosilicate matrix. However, in CBS glasses, the broad peak seems to split into two peaks, especially in sample of high calcium content. This may be caused by the existence of a second amorphous phase, and this will be discussed below.

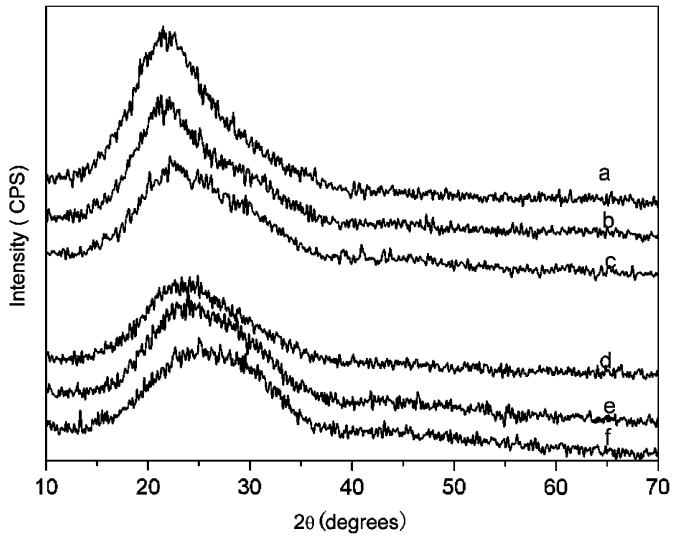


Fig. 1. WAXRD patterns of (a) C5BS90, (b) C15BS80, (c) C25BS70, (d) MC5BS90, (e) MC15BS80, and (f) MC25BS70.

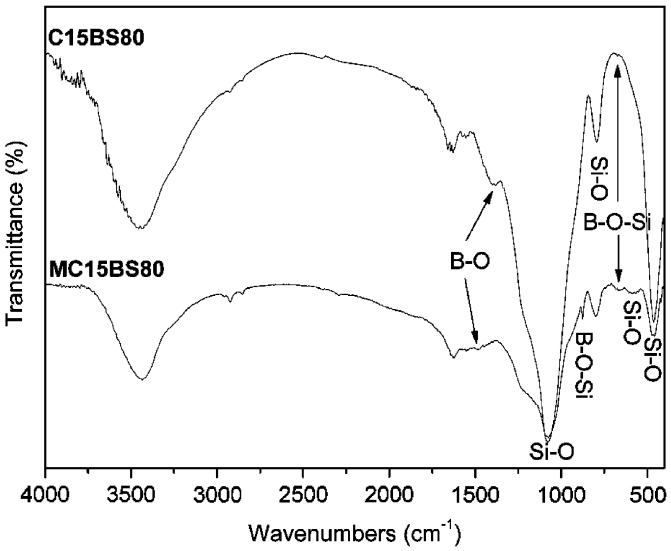


Fig. 2. FTIR spectra of MC15BS80 and C15BS80.

### 3.1.2. FTIR

Fig. 2 gives FTIR spectra of MC15BS80 and C15BS80. The absorption bands at ~1087, ~800, and ~460 $cm^{-1}$ are ascribed to Si–O bonds, while absorptions at 1630 and 3450 $cm^{-1}$ are due to bending and stretching mode of water [22]. The formation of Si–O–B linkage is confirmed by the absorption bands at ~910 and ~670 $cm^{-1}$ [23]. However, only a small peak at ~670 $cm^{-1}$ can be observed for C15BS80, suggesting that Si–O–B linkage is insufficient in conventional sol–gel-derived glasses. Due to the insufficient Si–O–B linkage, boron species may remain as individual domains in the framework, implying the heterogeneous nature of CBS glasses. Meanwhile, the intensity of the complex set of absorptions between 1300 and 1500 $cm^{-1}$, ascribed to B–O stretching vibrations in various boron environments [23], in C15BS80 is stronger than that in MC15BS80. This may also be caused by the existence of individual boron species in CBS glasses.

### 3.1.3. TG–DTA

Compositional homogeneity differences between the two kinds of glasses can also be demonstrated by TG–DTA curves (Fig. 3). According to the TG curve of MC15BS80, a slight mass loss appearing approximately before 373 K is attributed to the loss of the physical water adsorbed in the dried gel. As the heating process proceeds, a steep weight loss stage occurs between 473 and 673 K, which is most likely assigned to the simultaneous decomposition of inorganic precursors and block copolymers. The peak around 373 K in the DTA curve is ascribed to desorption of water. The pronounced exothermic peak observed between 373 and 773 K may be attributed to the thermal decomposition of block copolymer templates and inorganic precursors, in accordance with the TG data. The TG and DTA profiles for C15BS80 are different from MC15BS80.

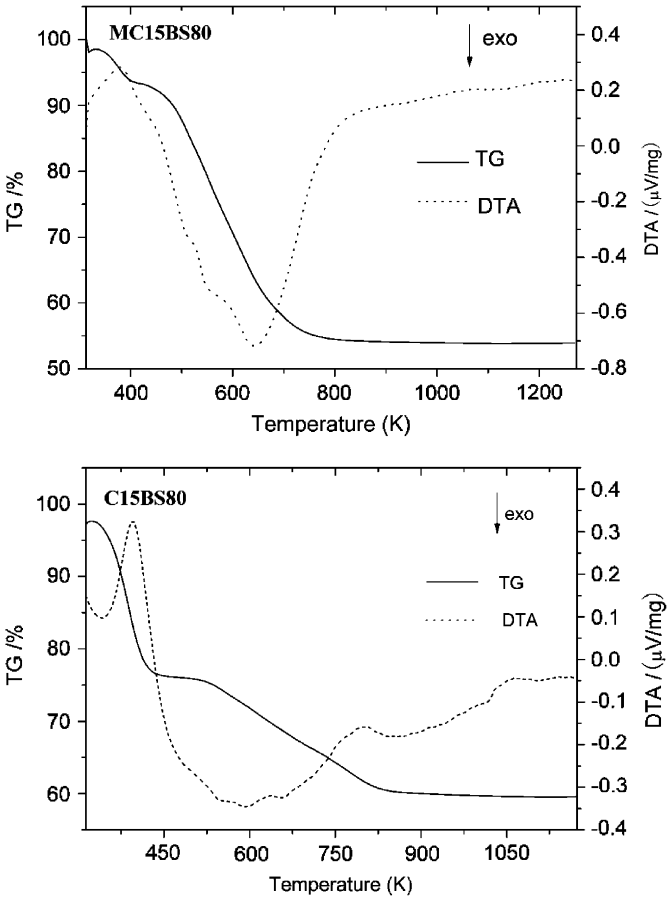


Fig. 3. TG–DTA curves of MC15BS80 and C15BS80.

For C15BS80, two large mass loss stages can be observed in the TG curve between 303 and 443 K as well as between 443 and 823 K. It is obvious that mass loss is much larger and the ending temperature is higher for C15BS80 at the first mass loss stage, for, in addition to desorption of physical adsorbed water, the decomposition of boric acid

into metaboric acid also occurs at this stage. It should be pointed out that the boric acid is formed during the sol–gel process and distributed randomly as individual domain in the gel framework [24]. The latter mass loss can be ascribed to the decomposition of inorganic precursors. It can be expected the final transformation of boric acid into boron oxide and melting of boron oxide also occur at this stage. Accordingly, the sharp peak around 395 K is caused by the decomposition of boric acid as well as desorption of water, the board exothermic peak ranging form 473 to 823 K refers to the decomposition of inorganic precursors. Differences in the TG–DTA curves suggest that MCBS are more homogeneous than CBS glasses.

Like other conventional sol–gel bioactive glasses ($CaO–SiO_2$, $CaO–P_2O_5–SiO_2$) [14,15], the sol–gel process for $CaO–B_2O_3–SiO_2$ system proceeds only by aggregation of silica particles, since the calcium nitrate and boron species are in soluble form in the gels. Namely, the silica species alone may aggregate and condense into the continuous gel system, while the calcium and boron species remain as individual domains in the gel framework. After calcination, boron species and calcium species may form a second amorphous phase. However, in the surfactant-templated glasses, due to the surfactant-templated mechanism, the inorganic species may be distributed homogeneously in the silica network at nanoscale (the wall thickness is calculated to be less than 4 nm, supposing that pores are hexagonal packed in small domains, wall thickness $= a_0 - D_{BJH}$, $a_0 = 2d_{100}/\sqrt{3}$), these species do not aggregate or become heterogeneous at high calcination temperature. Also, it was suggested that the interaction between the surfactants and inorganic species may provide MCBS glasses with more homogenous structure than that in conventional CBS glasses [25].

In addition, final Si/B is chemical analyzed to be 13.4 and 18.5 for C15BS80 and MC15BS80, respectively. It is obvious that the value of final Si/B for C15BS80 is smaller than that of MC15BS80. That is to say, more boron loss can be found in MC15BS80. Since boric species is distributed in the silica network at nanoscale in surfactant-templated gels, boron species are readily to volatilize at higher temperature. While in traditional glasses, boron species and calcium species exist in individual domains. During heat treatment, the melted boric oxide may form a second phase with calcium species, which is not easily to evaporate. So the final Si/B for C15BS80 is lower than that for MC15BS80. The chemical analysis can also demonstrate the chemical homogeneous advantage of MCBS glasses over CBS glasses.

### 3.2. Comparison of textural properties

Table 1 lists some textural parameters of MCBSs and CBSs. From the table, we can find that all the MCBSs samples have similar mean pore size of ~4 nm. However, pore size distribution (inset in Fig. 4) becomes broader with the increase of CaO contents and the decrease of $SiO_2$ contents. MCBSs possess relatively high BET surface areas and relatively high total pore volume. The data of BET surface areas and pore volume become diminished in MCBSs of high Ca/Si, showing that the mesoporous structure becomes partially collapsed. All the CBS glasses have quite low surface areas and pore volume, but the values get increased with increasing CaO contents.

Table 1
Textural parameters of MCBS and CBS glasses

| Sample | $S_{BET}$ ($m^2 g^{-1}$) | $D_{BJH}$ (nm) | Pore volume ($cm^3 g^{-1}$) |
|---|---|---|---|
| MC5BS90 | 321 | 4.1 | 0.386 |
| MC15BS80 | 284 | 4.2 | 0.331 |
| MC25BS70 | 205 | 4.1 | 0.256 |
| C5BS90 | 0.04 | – | 0 |
| C15BS80 | 0.16 | – | 0 |
| C25BS70 | 22.8 | 8.6 | 0.075 |

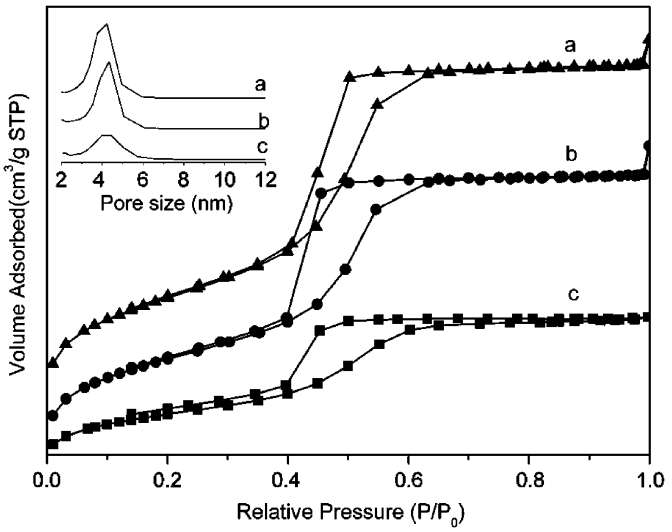


Fig. 4. The nitrogen adsorption and desorption isotherms and pore size distribution (inset) of (a) MC5BS90, (b) MC15BS80, and (c) MC25BS70.

The nitrogen adsorption and desorption isotherms (Fig. 4) of all the MCBS samples are type-IV isotherms with $H_2$-type hysteresis loop, typical of mesoporous materials with imperfect cylinder channels [26]. The imperfect mesopore ordering of MCBS can also be seen in SAXRD patterns (Fig. 5), where all the samples show only one strong peak, indicating a lower degree of channel packing order. Weakness and broadness of the peak with increasing Si/B is due to the partial collapse of the mesoporous structure. Arrangements of mesopores can be clearly seen in the HRTEM images. Fig. 6 shows the HRTEM images of MCBS glasses with different compositions. All the pictures depict a wormhole-like mesoporous structure. The glasses contain a large number of channels. The cylindrical- to hexagonal-shaped channels are regular in diameter (around 3–4 nm, in accordance with the nitrogen sorption isotherms results) and show short-range hexagonal-like packing, although they lack discernible long-range packing order. With increasing Ca/Si, the

mesoporous structure tends to be more disordered, confirming the partial collapse of the framework. Since $SiO_2$ is the net former of the framework, and CaO is the net modifier, the presence of $Ca^{2+}$ in the glass causes a discontinuity of the glassy network through the disruption of some Si–O–Si bonds. So increasing Ca/Si causes partial collapse of the framework.

Low porosity of CBS glasses is different from that of other conventional sol–gel-derived bioactive glasses ($CaO–SiO_2$, $P_2O_5–CaO–SiO_2$) [14,15]. These $CaO–SiO_2$ and $P_2O_5–CaO–SiO_2$ glasses are mesoporous and have relatively high surface areas, with disordered pores and widely distributed pore sizes. This is ascribed to the heterogeneity of conventional sol–gel-derived bioactive glasses. The calcium and phosphorous species remain as individual domains in the gel framework. When the gels are dried and calcined, the decomposition of calcium and phosphorous species may generate mesopores. However, in our case, boric acid is decomposed to metaboric acid and then to boron oxide after heat treatment. It is reasonably to expect that the melting boron oxide may fill in the pores that generated by decomposition of calcium species and form a second amorphous phase at higher temperature. However, when more calcium species exist in the gels, more pores are generated. Boron oxide is not enough to fill in all the pores, so porosity get increased in products of high Ca/Si.

On the contrary, in the surfactant-templated MCBS glasses, during the organic solvent evaporation process, progressively increasing block copolymer concentration leads to the self-assembly of silica-surfactant composite micelles and their further organization into mesophases. Removing of templates at high temperatures may lead to mesopores in MBSC glasses. Due to the effect of the surfactant, boric species is distributed homogeneously in the silica network at nanoscale, they do not aggregate at high temperature. After heat treatment, some of them may direct condense with the silica framework, and some may evaporate causing boron loss in the final product [27]. Since no formation of melting boron oxide, the mesopores will never be filled and then remain.

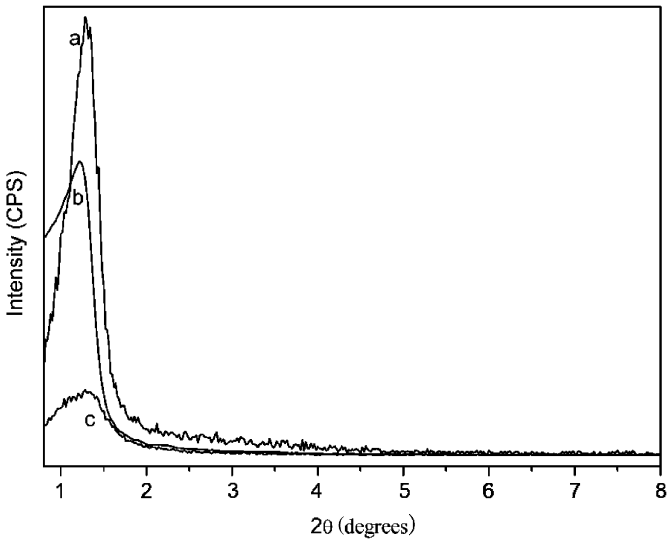


Fig. 5. SAXRD patterns of (a) MC5BS90, (b) MC15BS80, and (c) MC25 BS70.

### 3.3. Comparison of in vitro bioactivity

#### 3.3.1. ICP results

ICP plots (Fig. 7) show concentration change of chemical species (Ca, Si, and P) in SBF after MC15BS80 and C15BS80 soaking in SBF for 0–120 h. As can be seen, a very sharp increase in the Ca concentration takes place in the very first 8 h of the test for MC15BS80, but it then experiences a decrease and stabilizes at a certain value after 48 h. However, for the C15BS80, there is a slight increase in the Ca concentration for the first 8 h. Thereafter, almost no increase can be found. The plots of Si release show a common feature for the two samples: the Si concentration keeps increased as the soaking time increased, but the release rate slows down after 12 h of soaking. Also, it can be seen that more Si contents are released from MC15BS80. The change in the concentration of P also shows great difference for the two samples. For MC15BS80, there is a pronounced decrease with the soaking time prolonged, and stabilized after 48 h. In the case of C15BS80, there is only a slight decrease can be found until the end of the assay.

The increases in the calcium and silicon concentrations in SBF are attributed to dissolution of the calcium and

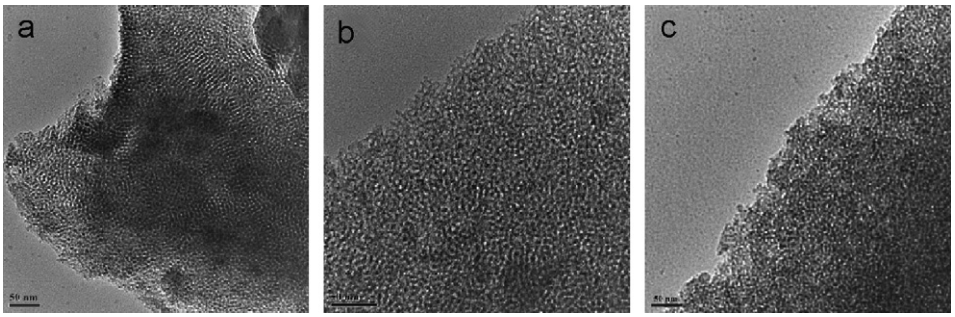


Fig. 6. HRTEM images of (a) MC5BS90, (b) MC15BS80, and (c) MC25BS70 (scale bars are 50 nm for all the pictures).

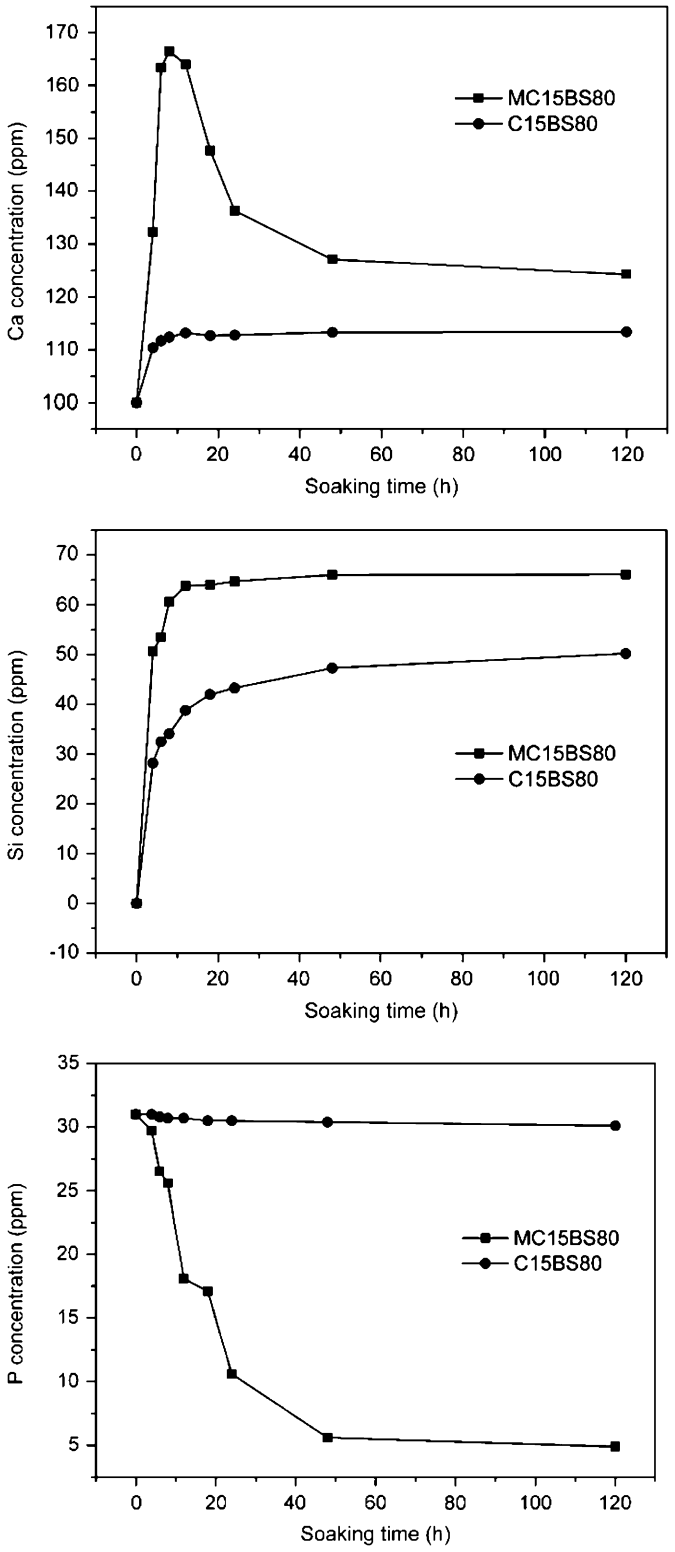


Fig. 7. Ca, Si, and P concentrations in SBF as a function of soaking time for MC15BS80 and C15BS80.

silicate ions from the glasses, and decrease in the phosphorus as well as later calcium decrease is attributed to formation of the amorphous phosphate and crystalline apatite on the surfaces of the glasses by consuming the phosphate and calcium ions from the SBF solutions. From the ICP plots comparisons, we can reach a conclusion that it is more powerful for MC15BS80 to release silicon and calcium ions and to consume phosphate ions from the SBF solutions.

### 3.3.2. FTIR

Fig. 8 shows FTIR spectra of MC15BS80 and C15BS80 after soaking in SBF for different time. The absorption band at 566 $cm^{-1}$ is due to presence of amorphous phosphate [28], after MC15BS80 soaking in SBF for 6 h. After 24 h, the band at 566 $cm^{-1}$ begins to split into a doublet at 566 and 601 $cm^{-1}$, characteristic of the phosphate group in the crystalline HAp phase [28–30]. However, after 120 h, new absorption bands at 879, 1430, and 1483 $cm^{-1}$ due to the carbonate group are also observed, indicating that the HAp phase is a carbonate-containing HAp similar to the apatite on the surface of bones in the body [29,30]. However, no above indicative bands are observed for C15BS80 after soaking in SBF for 120 h (Fig. 8e), suggesting that the induction time for the formation of amorphous apatite and the subsequent deposition rate of apatite on the surface of CBS glasses is much slower than that for MCBS glasses, a result which is in agreement with the inductively coupled plasma (ICP) atomic emission spectroscopy results.

### 3.3.3. SEM and TEM

SEM image of MC15BS80 before soaking (Fig. 9a) shows a smooth and homogenous surface. After immersion in SBF for 6 h (Fig. 9b), some sphere-like agglomerates were found spreading over the glass surface, due to the deposition of amorphous apatite. After soaking for 24 h,

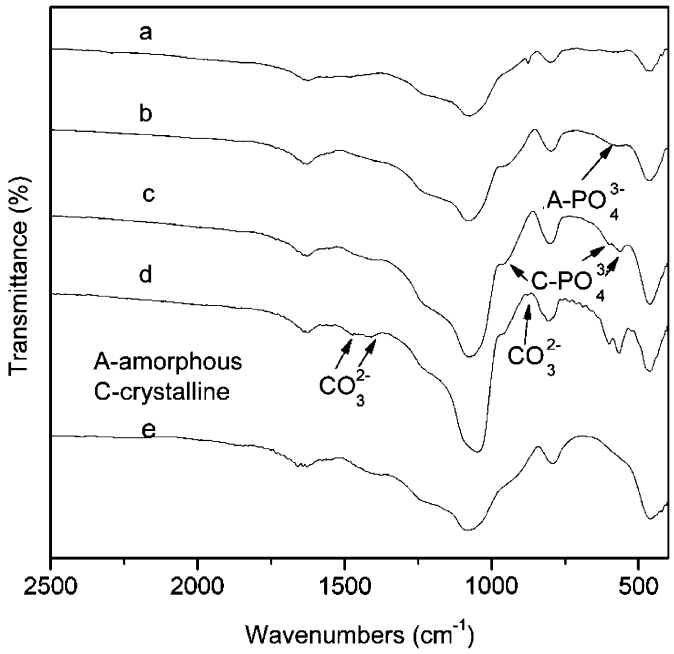


Fig. 8. FTIR spectra of MC15BS80 after soaking in SBF for (a) 0 h, (b) 6 h, (c) 24 h, and (d) 120 h. FTIR spectrum of C15BS80 after soaking in SBF for (e) 120 h.

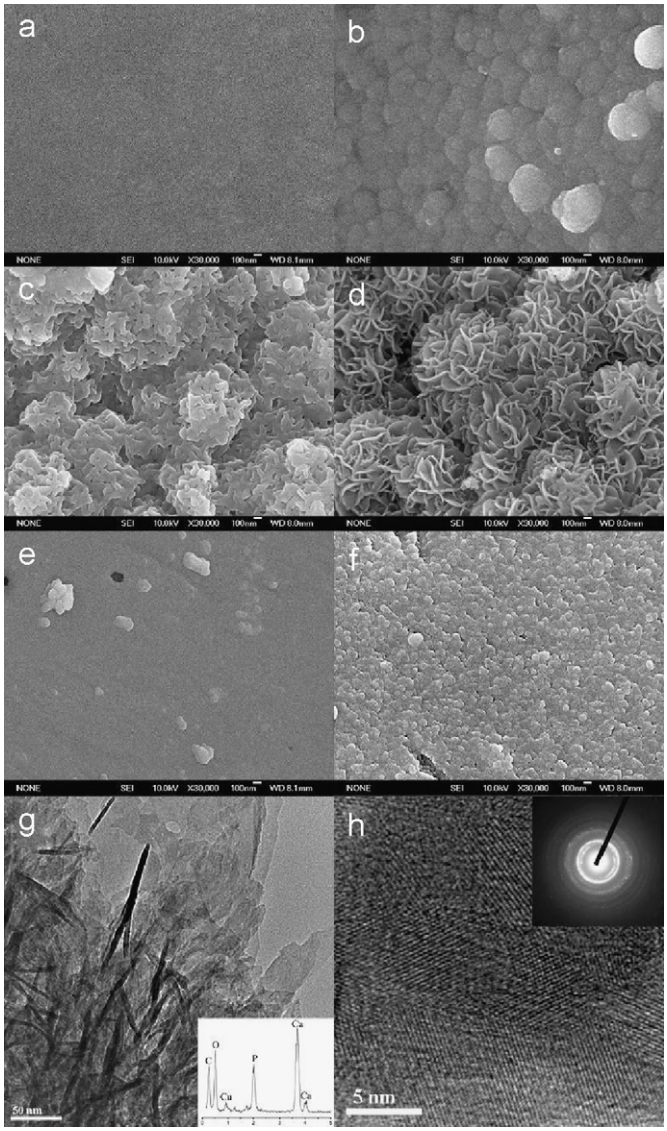


Fig. 9. SEM images of MC15BS80 after immersing in SBF for (a) 0 h, (b) 6 h, (c) 24 h, and (d) 120 h. SEM images of C15BS80 after immersing in SBF for (e) 0 h and (f) 120 h. TEM images of MC15BS80 after soaking in SBF for 120 h at different magnifications (g) and (h). The EDS result (inset in (g)) and SAED pattern (inset in (h)) of HCA deposited on MCBS glasses are also shown (the scale bars are 100 nm for (a), (b), (c), (d), (e), and (f), while 50 nm and 5 nm for (g) and (h), respectively).

newly formed worm-like HAp crystals can be seen (Fig. 9c). After 120 h (Fig. 9d), HAp crystals are turned to be plate-like with thin edges oriented perpendicular to the surfaces of glass powders. The plate-like HAp crystals aggregate in clusters to exhibit a rose-like morphology. Under TEM imaging (Fig. 9g), the HAp crystals are clearly seen to be aggregated together, with both plate- and rod-like morphology. In fact, the seeming nanorods are the thin edges of the plate-like HAp crystals. The crystallinity of the newly formed HAp phase is further confirmed by high-resolution TEM investigations (Fig. 9h). It is clear that HAp crystals have varying orientations, which in accordance with selected-area electron diffraction (SAED) patterns (inset in Fig. 9h), on which diffraction spots arranged in circular rings are present. Moreover, energy dispersive X-ray (EDX) analyses (inset in Fig. 9g) reveal that plate-like HAp crystals are calcium-deficient with an average Ca/P molar ratio of 1.50. Calcium-deficient HAp (d-HAp) can be represented by a general formula, $Ca_{10-x}(HPO_4)_x(PO_4)_{6-x}$ $(OH)_{2-x}$ [31], where $x$ ranges from 0 to 2, giving a Ca/P molar ratio between 1.67 and 1.33, while $x = 0$ corresponds to the stoichiometric HAp (s-HAp). d-HAp is of greater biological interest than s-HAp because biological HAp is calcium deficient, and plays some important roles in processes such as bone remodeling and formation [29,32]. However, for the C15BS80 glass, even after soaking for 120 h, no signs of formation of worm- or plate-like apatite can be found. Only rough surface can be observed, due to the dissolution of some soluble species.

In vitro bioactive tests show that wormhole-like MBCBS glasses with their larger pore volume and more accessible mesopore surface areas have much better in vitro bioactivity than CBS glasses. Due to high porosity of mesoporous glasses, they facilitate rapid and massive release of $Ca^{2+}$ ions from the glasses into the solution. This rapid release increases the $Ca^{2+}$ saturation and facilitates the formation of nucleation sites (Si–OH), and induces rapid deposition of apatite [14].

## 4. Conclusions

Wormhole-like mesoporous MCBS glasses are superior to conventional sol–gel glasses in compositional homogeneity, textural properties and in vitro bioactivity. In conventional CBS glasses, the silica species alone aggregate and condense into the continuous gel system, while the calcium and boron species remain as individual domains in the gel framework. Because of the heterogeneity, melting boron oxide might fill in the pores that should have been generated by decomposition of calcium species. Due to the effect of the surfactant in MCBS glasses, the inorganic species may be distributed homogeneously in the silica network at nanoscale, these species do not aggregate or become heterogeneous at high calcination temperature. Since no aggregation of boron oxide during heat treatment, wormhole-like mesopores resulting from the removal of self-assembled surfactant remain. Due to the high porosity of MCBS glasses, they exhibit better in vitro bioactivity. The combination of high compositional homogeneity and the superior in vitro bioactivity, together with the porous nature, properties that are useful for carrying drugs and immobilizing enzymes, make the wormhole-like MCBS glasses promising for applications in clinical orthopedics, controlled drug delivery, tissue engineering, etc.

## Acknowledgments

We would like to thank the financial support of the National Natural Science Foundation of China (No.

50372080). We would also like to thank Mr. Manjiang Dong for $N_2$ sorption measurements.

## References

[1] L.L. Hench, R.J. Splinter, W.C. Allen, T.K. Greenlee, J. Biomed. Mater. Res. 5 (1972) 117–141.
[2] L.L. Hench, J. Am. Ceram. Soc. 74 (1991) 1487–1510.
[3] P. Li, C. Ohtsuki, T. Kokubo, K. Nakanishi, N. Soga, T. Nakamura, T. Yamamuro, J. Mater. Sci.: Mater. Med. 4 (1993) 127–131.
[4] M.M. Pereira, A.E. Clark, L.L. Hench, J. Biomed. Mater. Res. 28 (1994) 693–698.
[5] L.L. Hench, J.M. Polak, Science 295 (2002) 1014–1017.
[6] T. Kokubo, Biomaterials 12 (1991) 155–163.
[7] C. Ohtsuki, T. Kokubo, T. Yamamuro, J. Non-Cryst. Solids 143 (1992) 84–92.
[8] C. Ohtsuki, Y. Kobayashi, K. Tsuru, A. Osaka, J. Soc. Mater. Sci. Jpn. 44 (1995) 693–699.
[9] H.S. Ryu, J.K. Lee, J.H. Seo, H. Kim, K.S. Hong, D.J. Kim, J.H. Lee, D.H. Lee, B.S. Chang, C.K. Lee, S.S. Chung, J. Biomed. Mater. Res. Part A 68A (2004) 79–89.
[10] J.H. Lee, C.K. Lee, B.S. Chang, H.S. Ryu, J.H. Seo, S. Hong, H. Kim, J. Biomed. Mater. Res. Part A 77A (2006) 362–369.
[11] H.S. Ryu, J.H. Seo, H. Kim, K.S. Hong, H.J. Park, D.J. Kim, J.H. Lee, D.H. Lee, B.S. Chang, C.K. Lee, Bioceramics 15, Trans Tech Publications Ltd., Zurich-Uetikon, 2003, p. 261.
[12] L.L. Hench, J.K. West, Chem. Rev. 90 (1990) 33–72.
[13] P. Saravanapavan, L.L. Hench, J. Non-Cryst. Solids 318 (2003) 1–13.
[14] M. Vallet-Regi, C.V. Ragel, A.J. Salinas, Eur. J. Inorg. Chem. (2003) 1029–1042.
[15] M. Jokinen, H. Rahiala, J.B. Rosenholm, T. Peltola, I. Kangasniemi, J. Sol–Gel Sci. Technol. 12 (1998) 159–167.
[16] S.A. Bagshaw, E. Prouzet, T.J. Pinnavaia, Science 269 (1995) 1242–1244.
[17] P.T. Tanev, T.J. Pinnavaia, Science 267 (1995) 865–867.
[18] T.P. Xiu, Q. Liu, J.C. Wang, J. Mater. Chem. 16 (2006) 4022–4024.
[19] T.R. Pauly, Y. Liu, T.J. Pinnavaia, S.J.L. Billinge, T.P. Rieker, J. Am. Chem. Soc. 121 (1999) 8835–8842.
[20] W.Z. Zhang, T.R. Pauly, T.J. Pinnavaia, Chem. Mater. 9 (1997) 2491–2498.
[21] T.P. Xiu, Q. Liu, J.C. Wang, Chem. Lett. 36 (2007) 730–731.
[22] J.C. Wang, Q. Liu, Chem. Commun. (2006) 900–902.
[23] A.S. Tenney, J. Wong, J. Chem. Phys. 56 (1972) 5516–5523.
[24] A.D. Irwin, J.S. Holmgren, T.W. Zerda, J. Jonas, J. Non-Cryst. Solids 89 (1987) 191–205.
[25] X.X. Yan, H.X. Deng, X.H. Huang, G.Q. Lu, S.Z. Qiao, D.Y. Zhao, C.Z. Yu, J. Non-Cryst. Solids 351 (2005) 3209–3217.
[26] K.S.W. Sing, D.H. Everett, R.A.W. Haul, L. Moscou, R.A. Pierotti, J. Rouquerol, T. Siemieniewska, Pure Appl. Chem. 57 (1985) 603–619.
[27] T.P. Xiu, Q. Liu, J.C. Wang, J. Mater. Res. 22 (2007) 1834–1838.
[28] A. Lopez-Noriega, D. Arcos, I. Izquierdo-Barba, Y. Sakamoto, O. Terasaki, M. Vallet-Regi, Chem. Mater. 18 (2006) 3137–3144.
[29] Q.H. Shi, J.F. Wang, J.P. Zhang, J. Fan, G.D. Stucky, Adv. Mater. 18 (2006) 1038–1042.
[30] X.X. Yan, C.Z. Yu, X.F. Zhou, J.W. Tang, D.Y. Zhao, Angew. Chem. Int. Ed. 43 (2004) 5980–5984.
[31] S.J. Joris, C.H. Amberg, J. Phys. Chem. 75 (1971) 3172–3178.
[32] A.S. Posner, Physiol. Rev. 49 (1969) 760–792.